

# Na<sub>3</sub>V<sub>2</sub>(PO<sub>4</sub>)<sub>3</sub>/C/Ag nanocomposite materials for Na-ion batteries obtained by the modified Pechini method

Andrey Chekannikov<sup>1,2</sup> · Roman Kapaev<sup>3</sup> · Svetlana Novikova<sup>3</sup> ·  
Nataliya Tabachkova<sup>4</sup> · Tatiana Kulova<sup>2</sup> · Alexander Skundin<sup>2</sup> · Andrey Yaroslavtsev<sup>3</sup>

Received: 22 October 2016 / Revised: 25 January 2017 / Accepted: 27 January 2017 / Published online: 14 February 2017  
© Springer-Verlag Berlin Heidelberg 2017

**Abstract** Nanocomposite materials, Na<sub>3</sub>V<sub>2</sub>(PO<sub>4</sub>)<sub>3</sub>/C and Na<sub>3</sub>V<sub>2</sub>(PO<sub>4</sub>)<sub>3</sub>/C/Ag, were synthesized by a modified Pechini method. Their properties were characterized with the use of the X-ray diffraction analysis, scanning electron microscopy, transmission electron microscopy, thermogravimetric analysis, elemental analysis, Raman spectroscopy, impedance spectroscopy, and charge-discharge tests as cathode materials for sodium-ion batteries. The discharge capacity of Na<sub>3</sub>V<sub>2</sub>(PO<sub>4</sub>)<sub>3</sub>/C obtained at 600 °C was 116.1 and 75 mAh g<sup>-1</sup> at a current density of 11 (0.1 C) and 110 mA g<sup>-1</sup> (1 C) in the potential range of 2.7–3.8 V. The high capacity values for fast charge/discharge were achieved as a result of heat treatment by two steps and incorporation of appropriate amount of silver particles into Na<sub>3</sub>V<sub>2</sub>(PO<sub>4</sub>)<sub>3</sub>/C nanocomposite. The discharge capacities of thus obtained Na<sub>3</sub>V<sub>2</sub>(PO<sub>4</sub>)<sub>3</sub>/C with 0.2 wt% of Ag were 117.2, 112.5, and 83.5 mAh g<sup>-1</sup> at the current densities of 11, 110, and 880 mA g<sup>-1</sup>. This experimental evidence

reveals the great potential of NVP/C/Ag synthesized by the modified Pechini method as cathode materials for the production of sodium-ion batteries.

**Keywords** Na<sub>3</sub>V<sub>2</sub>(PO<sub>4</sub>)<sub>3</sub> · Cathode materials · Sodium-ion batteries

## Introduction

Lithium-ion batteries (LIBs) are widely used as portable energy sources. However, due to scarcity of the lithium resources in the world, the development of alternative devices beyond LIB is necessary. Sodium is the 6th abundant and non-toxic alkali element [1], which can be implemented in insertion-based batteries. The electrochemical principles of sodium-ion batteries (SIBs) are identical to those of lithium-ion batteries [2]. Hence, considerable attention has been paid to find suitable electrode materials for SIBs. As compared with the LIBs, SIBs offer a low-cost and environmentally friendly alternative [3, 4]. Taking into account the fact that molten sodium batteries (Na-S and zero emission battery research activity (ZEBRA) cells) operating at 300–350 °C [5, 6] are unsafe, the research efforts have been focused on the systems operating at room temperature.

At the present time, diverse positive and negative electrode materials, including layered oxides, polyanionic compounds, carbon-based electrode materials, Ti-based compounds, Na alloys, and organic compounds, are used in the Na-ion batteries [7]. However, due to larger radius of sodium ions, the diffusion rate decreases and, upon intercalation and extraction processes, structural changes in the electrode occur.

Sodium vanadium(III) phosphate, Na<sub>3</sub>V<sub>2</sub>(PO<sub>4</sub>)<sub>3</sub> (NVP), is characterized by the (NASICON)-type framework structure with big-sized interstitial space where sodium ions may

**Electronic supplementary material** The online version of this article (doi:10.1007/s10008-017-3524-4) contains supplementary material, which is available to authorized users.

✉ Svetlana Novikova  
novikova@igic.ras.ru

<sup>1</sup> Skolkovo Institute of Science and Technology, Nobel Street 3, Moscow 143026, Russia

<sup>2</sup> Frumkin Institute of Physical Chemistry and Electrochemistry, The Russian Academy of Sciences, Leninsky prospect 31-4, Moscow 119071, Russia

<sup>3</sup> Kumakov Institute of General and Inorganic Chemistry, The Russian Academy of Sciences, Leninsky prospect 31, Moscow 119991, Russia

<sup>4</sup> National University of Science and Technology, Leninsky prospect 4, Moscow 119991, Russia

diffuse [8–14]. The abbreviation means Na super ionic conductor due to high  $\text{Na}^+$  ionic conductivity provided by the 3D open framework [14]. NVP is composed of corner-shared  $\text{VO}_6$  octahedra and  $\text{PO}_4$  tetrahedra with large tunnels, and it is able to accommodate sodium ions [15]. As a cathode material, NASICON NVP offers several advantages: (1) a relatively high theoretical specific capacity which is equal to  $117.6 \text{ mAh g}^{-1}$ ; (2) a high discharge potential (plateau at about 3.4 V vs  $\text{Na}^+/\text{Na}$  which is higher than the plateaus of most cathode materials for the Na-ion batteries; (3) a long cycle life; (4) a relatively low-cost, thermal, and structural stability; and (5) non-toxicity [16]. However, its electronic conductivity is very low [17–19]. To overcome this disadvantage, diverse approaches were proposed, including coating with a conductive carbon [20] and doping with metal ions [21], minimization of particle size [22], and control over morphology (nanoparticles [23], porous materials [24], double carbon-embedding nanosized materials [25], nanotubes [26, 27], and nanofibers [22]), which provide higher effective reaction areas and shortened diffusion paths for electrons and sodium ions. An additional increase in the electrical conductivity of the coating can be achieved by modifying the particles of cathode materials by metal nanoparticles [28, 29].

Numerous methods for the preparation of NVP are described. The benefits of the solid-state synthesis are concerned with its simplicity. However, this method requires the use of relatively long-time and high temperature annealing [23, 30]. The advantages of liquid-phase methods are related to mixing of reagents at the molecular level in the solutions. Hence, this process takes place at lower annealing temperatures or time and allows development of smaller sized particles [31, 32]. Promising results, which outshine even lithium cathodes under high rate conditions, were obtained by Zhu et al. for NVP/C using soft chemistry-based double carbon-embedding approach which combines the advantages of carbon-coating nanosized particles with the presence of a porous carbon matrix [25].

The aim of this study was to provide and optimize a simple procedure for preparation of NVP nanomaterial coated with a carbon shell by means of the Pechini method with silver nanoparticles introduction into NVP/C composites and to study their charge-discharge behavior as cathode materials for SIBs.

## Experimental

### *Preparation of the samples*

The NVP/C nanocomposites were synthesized by the modified Pechini method. Analytical grade reagents were used.  $\text{V}_2\text{O}_5$ , oxalic acid,  $\text{NaH}_2\text{PO}_4 \cdot 2\text{H}_2\text{O}$ , and citric acid were mixed in a molar ratio of 1:6:3:2, and the mixture was placed into a glass of water and ethylene glycol mixed in a volume ratio of 3:7. The mixture was kept upon heating (50–80 °C)

and stirring until the solid phase was completely dissolved.  $\text{V}_2\text{O}_5$  was used as one of the most available vanadium-containing reagent. Oxalic acid was used as a chelating and reducing agent. After the  $\text{V}_2\text{O}_5$  was completely dissolved, the formation of a dark blue solution was observed. The solution was heated up to 300 °C and kept for 2 h. The residue was grinded and annealed in argon atmosphere for 10 h at 600–800 °C.

The materials containing silver nanoparticles, NVP/C/Ag, were prepared in a similar way with addition of  $\text{AgNO}_3$  (0.1–5 wt% relative to NVP) to a solution of precursors.

The calcination temperature of the sample is given as the final part of the sample name (NVP/C-600, NVP/C/Ag-600, NVP/C-800). The samples that were annealed first at 600 °C for 10 h then heated at 800 °C for 2 h are denoted as NVP/C-600-800, NVP/C/Ag-600-800.

### *Characterization of the samples*

The X-ray diffraction (XRD) analysis was performed using a Rigaku D/MAX 2200 diffractometer ( $\text{CuK}_\alpha$  radiation, 40 kV/30 mA) with  $\Theta/2\Theta$  geometry ( $2\Theta = 10^\circ\text{--}60^\circ$ , scanning rate was  $4^\circ/\text{min}$ ). The XRD data were analyzed using the Rigaku application data processing.

Microstructure of the samples was studied on a Carl Zeiss NVision 40 scanning electron microscope (SEM) (micrographs were collected at an accelerating voltage of 1 kV), scanning electron microscope JSM-6480LV Jeol, equipped with an energy-dispersive X-ray (EDX) analyzer operating at an accelerating voltage of 15 kV and with the help of transmission electron microscope (TEM) Jeol JEM 2100 at an acceleration voltage of 200 keV.

The conductivity was measured using a two-probe method on a 2B-1 universal bridge at the alternating current (ac) in a frequency range 10 Hz to 2 MHz. Circular pressed pellets ( $d = 6 \text{ mm}$ ,  $h = 1 \text{ mm}$ ) with silver electrodes were used for the conductivity measurements. The pellets were prepared at a pressure of 500 MPa. The experiments were performed at room temperature. The conductivity was estimated from the resistance obtained by the extrapolation of the impedance spectrum onto the active resistance axis.

Thermogravimetric analysis (TGA) was performed using a thermobalance Netzsch TG 209 in platinum crucibles in the temperature range 25–600 °C in air atmosphere with a heating rate of  $10^\circ \text{ min}^{-1}$ . The composition of evolved gases was identified by a mass spectrometer Netzsch Aeolos QMS 403 C.

The carbon content was estimated using an EuroEA 3000 carbon, hydrogen, nitrogen, and sulfur (CHNS) analyzer.

The Raman spectroscopic measurements were conducted on a DXRxi Raman imaging microscope (Thermo Fisher Scientific) equipped with a  $\times 10$  optical zoom and green solid-state laser (532 nm). The laser spot size was about

1  $\mu\text{m}$ . The number of accumulations was 50 at a low laser intensity (0.8 mW); exposure time was 1 s.

### Electrochemical measurements

Electrode paste was prepared by mixing NVP/C or NVP/C/Ag as an active material (70%), a conducting carbon black (Timcal, Belgium) (20%), and a binding agent [poly(vinylidene fluoride) (Aldrich)] (10%) dissolved in the water-free *N*-methyl-2-pyrrolidone [Aldrich, 50 ppm H<sub>2</sub>O]. The prepared paste was deposited as a thin layer onto an oil-free aluminum foil (a current collector) and was dried at a temperature of 100 °C. Then, the electrode was pressed at a pressure of 100 MPa and dried in vacuum at a temperature of 120 °C for 8 h. The amount of NVP/C or NVP/C/Ag on the electrode was 5 mg cm<sup>-2</sup>.

Electrochemical measurements were performed in the sealed three-electrode cells containing a working electrode (NVP/C or NVP/C/Ag), an auxiliary electrode (Na), and a reference electrode (Na). Surface area of the working electrode was 2.25 cm<sup>2</sup>. The cells were assembled in a glove box under the dry argon atmosphere with a moisture content of about 10 ppm. A non-woven polypropylene separator (NPO UFIM, Russia) was sandwiched between the electrodes. As an electrolyte, we used 1 M NaPF<sub>6</sub> solution in a mixture of ethylene carbonate (EC) and propylene carbonate (PC) (1:1). Water content in the electrolyte was measured by the coulometric Karl Fischer titration, and this value did not exceed 15 ppm. Electrochemical cycling of the cells was performed over the potential window of 2.7–3.8 V using a ZRU 50 mA–10 V charge-discharge system (NTT Buster JSC, Russia). The tests were performed under the galvanostatic mode at a current density of 11, 55, 110, 220, 440, 880, 1600, and 2640 mA g<sup>-1</sup>. Specific capacity was calculated per unit weight of the NVP. Cyclic voltammetry was performed using an Elins P-8NANO (TzVA) potentiostat (Chernogolovka, Russia); potential scanning rates were 0.05, 0.1, 0.2, 0.4, and 0.8 mV s<sup>-1</sup> over the potential window ranging from 2.5 to 4.1 V.

## Results and discussion

### Composition and morphology

The XRD patterns of all obtained NVP/C samples show a single rhombohedral NASICON phase (compared with those of card no. 53-0018 ICDD PDF2) which is well-indexed in the *R*- $3c$  space group according to [18, 33–35] (Fig. 1, and Table 1). The use of the Pechini method allows to decrease the annealing temperature required for obtaining a crystalline sample and obtain crystalline sample already at 600 °C (Fig. 1a). For example, attempts to synthesize Na<sub>3</sub>V<sub>2</sub>(PO<sub>4</sub>)<sub>3</sub> samples at 600 °C by precursors mixed as solid phases yield

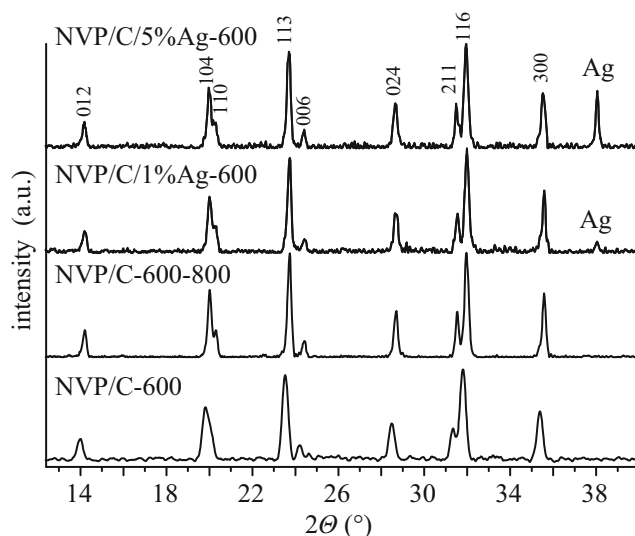


**Fig. 1** The XRD patterns of NVP/C-600, NVP/C-600-800, and NVP/C/Ag-600 with Ag content of 1 and 5 wt%

amorphous products [23]. The XRD patterns of NVP/C/Ag with Ag content 1–5% also exhibit a peak corresponding to silver in the  $2\theta$  region of  $\sim 38^\circ$  (Fig. 1). The amount of carbon was estimated to be about 5.5 wt% from the weight loss in an air atmosphere (Supplementary Fig. S1). According to the CHNS analysis, the content of carbon in the NVP/C samples was  $\sim 8$  wt%. This value seems more valid in our case.

The well-pronounced band peaked at  $\sim 1591$  cm<sup>-1</sup> in the Raman spectra of NVP/C (Supplementary Fig. S2) can be assigned to the G-band, and the band at  $\sim 1354$  cm<sup>-1</sup> can be assigned to the D-band of graphite [36–38]. The  $I_D/I_G$  ratio is widely used as the reference parameter for the quality assessment of the carbon coating because this parameter correlates with the structure of the involved carbon [37–41]. In the prepared materials, this parameter is low and is about 0.95. So, one can conclude that carbon coating of obtained samples primarily comprises the graphite structure.

The Pechini method involves polycondensation of ethylene glycol and citric acid, which leads to the formation of a polymeric matrix that prevents the growth of particles. Further heat treatment of this precursor allows preparation of the materials with a high level of homogeneity and dispersion [42–44]. Dimensions of primary particles calculated through the Scherrer equation were summarized in Table 1. The increase in the annealing temperature from 600 to 800 °C leads to the substantial increase in the size of primary particles. While, for the NVP/C-600-800 annealed first at 600 °C and after that heated at 800 °C, the relatively low particle size was observed (Table 1).

Morphology of NVP/C was further investigated by scanning electron microscopy and transmission electron microscopy technologies. TEM images show that the grain sizes are around 20–60 nm for NVP/C-600 (Fig. 2a, b), 50–300 nm for NVP/C-800 (Fig. 2c), 30–80 nm for NVP/C-600-800

**Table 1** Unit cell parameters and particles sizes of  $\text{Na}_3\text{V}_2(\text{PO}_4)_3$ 

Sample	Preparation condition	Unit cell parameters		Particle size, nm (XRD)	Particle size, nm (TEM)
		$a$ , Å	$c$ , Å		
NVP/C-600	600 °C for 10 h	8.720(7)	21.796(3)	$30 \pm 1$	20–60
NVP/C-800	800 °C for 10 h	8.711(4)	21.785(1)	$70 \pm 2$	50–300
NVP/C-600-800	600 °C for 10 h + 800 °C for 2 h	8.717(2)	21.798(1)	$40 \pm 1$	30–80
NVP/C/Ag-600-800	600 °C for 10 h + 800 °C for 2 h	8.719(2)	21.800(1)	$38 \pm 2$	30–80

(Fig. 2d), and NVP/C/Ag-600-800 (Fig. 2e, f). The particle sizes observed by TEM are summarized in Table 1. The particles are coated with the carbon layer with the typical

thickness about 4–8 nm. The high-resolution TEM (HRTEM) images of NVP/C (Fig. 2b, d) reveal clear atomic layers with d-spacings of around 0.31, 0.37, and 0.62 nm,

**Fig. 2** HRTEM images of NVP/C-600 (a, b), NVP/C-600-800 (d), and of NVP/C/Ag-600-800 (f); TEM-image of NVP/C-800 (c) and of NVP/C/Ag-600-800 (e)

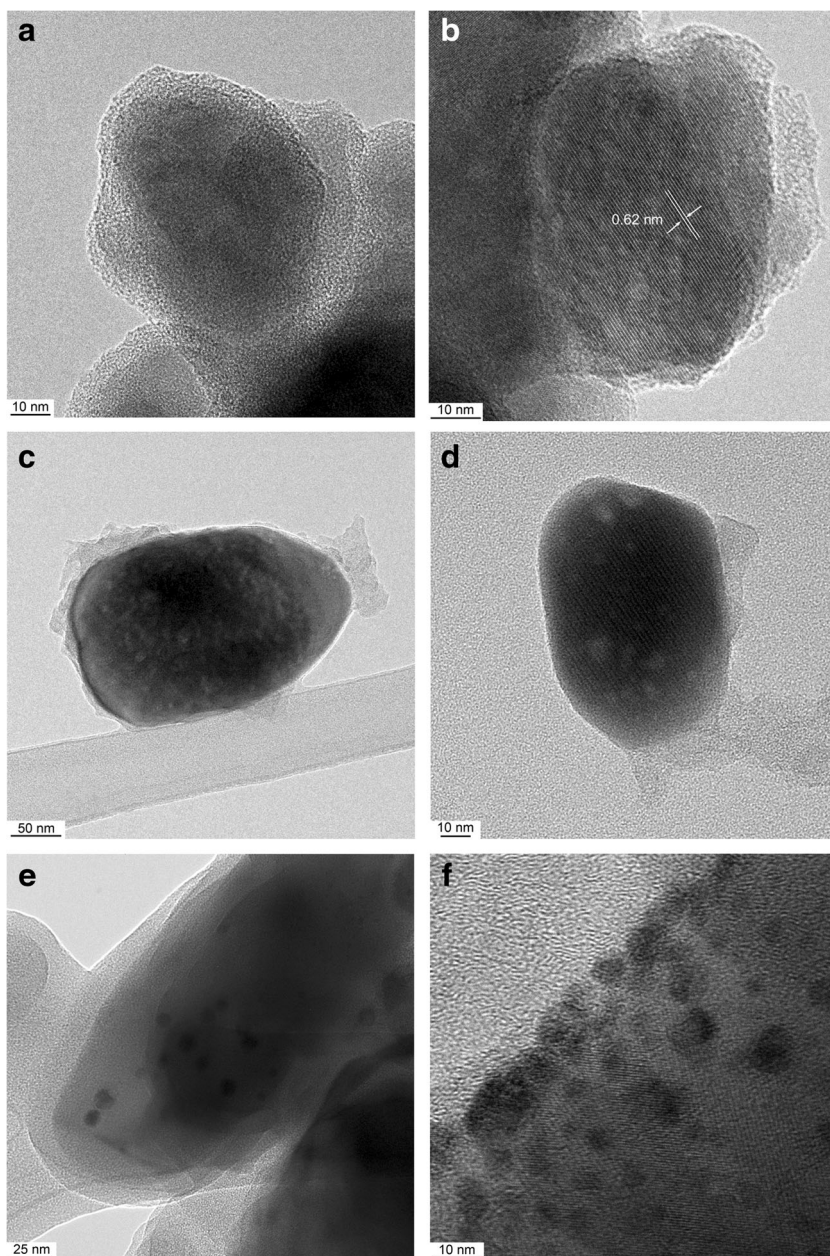
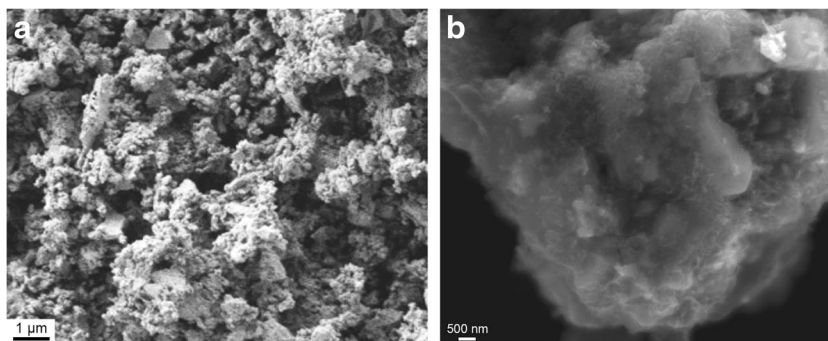


**Fig. 3** The SEM micrographs of NVP/C-600 (a) and NVP/C/0.2Ag-600-800 (b)



which correspond to the (024), (113), and (012) (Fig. 2b) lattice planes. The electron diffraction data confirmed crystalline NVP formation. TEM images of NVP/C/Ag-600-800 contain dark dots that correspond to the silver nanoparticles (Fig. 2e, f) with the sizes about 3–10 nm.

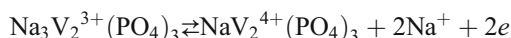
The primary NVP particles are agglomerated into conglomerates with dimensions varying from 200 nm to 5 μm according to SEM data (Fig. 3). Silver nanoparticles are not visualized in SEM micrographs of NVP/C/Ag due to the small size (Fig. 3b). The content of Na, V, P, and O practically corresponds to the composition  $\text{Na}_3\text{V}_2(\text{PO}_4)_3$  according to EDX analysis (Fig. 4a). In the case of NVP/C/Ag composites, Ag content was confirmed by EDX analysis (Fig. 4b).

#### Electrochemical characteristics

To evaluate the electrochemical characteristics of the synthesized NVP/C and NVP/C/Ag as cathode materials for the Na-ion batteries, electrochemical tests were conducted. Charge-discharge processes of NVP/C take place via the two-phase mechanism, and this scenario is proved by the X-ray phase analysis data (Fig. 5). According to the X-ray data for electrode materials, upon charging, the intensity of the peaks corresponding to the initial NVP gradually decreases, whereas, the intensity of the peaks corresponding to  $\text{NaV}_2(\text{PO}_4)_3$  (isostructural  $\text{NaTi}_2(\text{PO}_4)_3$  card 33-1296 ICDD PDF-2) increases (Fig. 5). That is why, charge-discharge processes take place at a substantially constant voltage due to the charge/

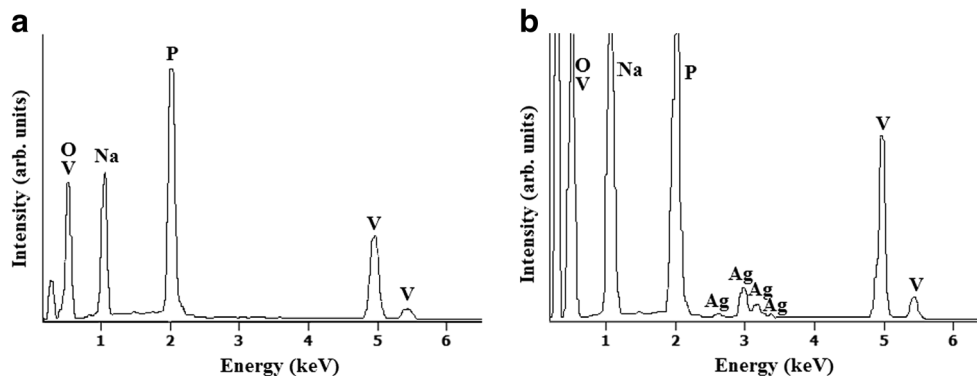
discharge through the phase transition in accordance with the Gibbs' phase rule and well-pronounced charge and discharge plateaus can be observed in the charge-discharge curves (Fig. 6). For the initial NVP-600, the unit cell parameters are the following:  $a = 8.720(7) \text{ \AA}$ ,  $c = 21.796(3) \text{ \AA}$ ; for the charged modification of  $\text{NaV}_2(\text{PO}_4)_3$ , these values decrease to  $a = 8.435(2) \text{ \AA}$ ,  $c = 21.499(1) \text{ \AA}$ . Upon sodium ions deintercalation, the unit cell volume decreases by less than 8%—from 1435(2) to 1324(1)  $\text{ \AA}^3$ .

Galvanostatic charge-discharge cycling at a current density of  $11 \text{ mAh g}^{-1}$  (0.1 C) has shown that discharge capacity for NVP/C-600 upon the first charge-discharge cycle is  $116.1 \text{ mAh g}^{-1}$  (Table 2, Figs. 6a, 7). This value corresponds to the intercalation-extraction of two sodium ions per NVP according to the following reaction:



The dependence of the discharge capacity on the current density (Fig. 6a, Fig. 7, Table 2) shows that, as the current density increases by an order of magnitude from 11 (0.1 C) to  $110 \text{ mA g}^{-1}$  (1 C), the discharge capacity of NVP/C-600 decreases to  $75 \text{ mAh g}^{-1}$ . In this case, the recovery of low current density suggests that this decrease is reversible. This fact can be due to the low electronic conductivity of carbon layer, which is not formed completely at such temperatures. Conductivity values  $\sigma$  ( $\text{S cm}^{-1}$ ) of the NVP/C and NVP/C/Ag samples measured by AC impedance spectroscopy are

**Fig. 4** EDX spectra of NVP/C/600-800 (a) and NVP/C/0.2Ag-600-800 (b) samples



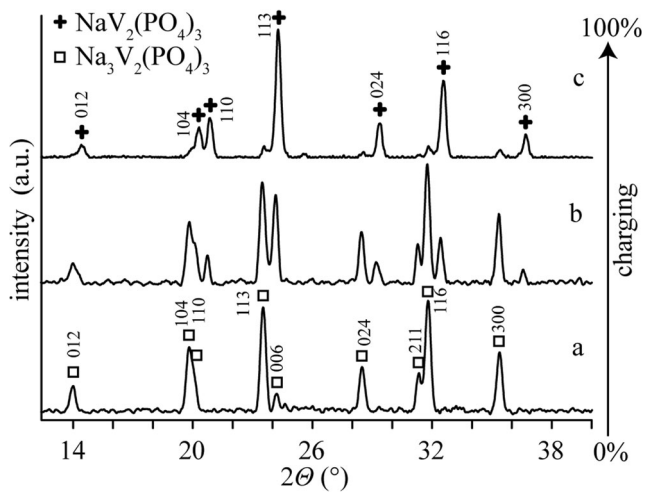


**Fig. 5** The XRD patterns of NVP/C-600 for charge degrees 0 (a), ~48 (b), and ~98% (c)

presented in Table 2. Annealing temperature increase results in the significant conductivity increase. Calcination at 800 °C leads to lower initial discharge capacity (Table 2, NVP/C-800) without improvement in capacities at high cycling rate. This fact can be explained by the increase in the particle sizes of the sample NVP-800 (Fig. 2c). However, NVP/C annealing first

at 600 °C with post heating at 800 °C (NVP/C-600-800) leads to the high initial discharge capacity and improved rate capability (Fig. 7, Table 2).

As was shown previously for LiFePO<sub>4</sub>/C, the formation of the composites of cathode material and small amount of silver nanoparticles increases electrical conductivity [29]. An additional increase in the conductivity can be achieved by insertion of silver nanoparticles into the composites (Table 2). The effect of silver incorporation became more noticeable at charge-discharge processes at high current densities. The significant decrease of polarization at current densities is >11 mA g<sup>-1</sup> and the lower rates of capacity decrease with an increase in current density were observed both for the samples NVP/C/Ag-600 and NVP/C/Ag-600-800 compared to those of NVP/C-600 and NVP/C-600-800, respectively (Fig. 6a–d, Table 2). However, the initial discharge capacity of NVP/C/Ag-600 was lower and decreased with Ag content increase. The best results were obtained using the combination of optimization of heat treatment condition and silver incorporation (<1 wt%), which results in a significantly lower polarization and higher capacities at fast charge/discharge. The best result was obtained for NVP/C/Ag-600-800 material with Ag content of 0.2 wt%. Its capacities were 117.2, 112.5, and 83.5

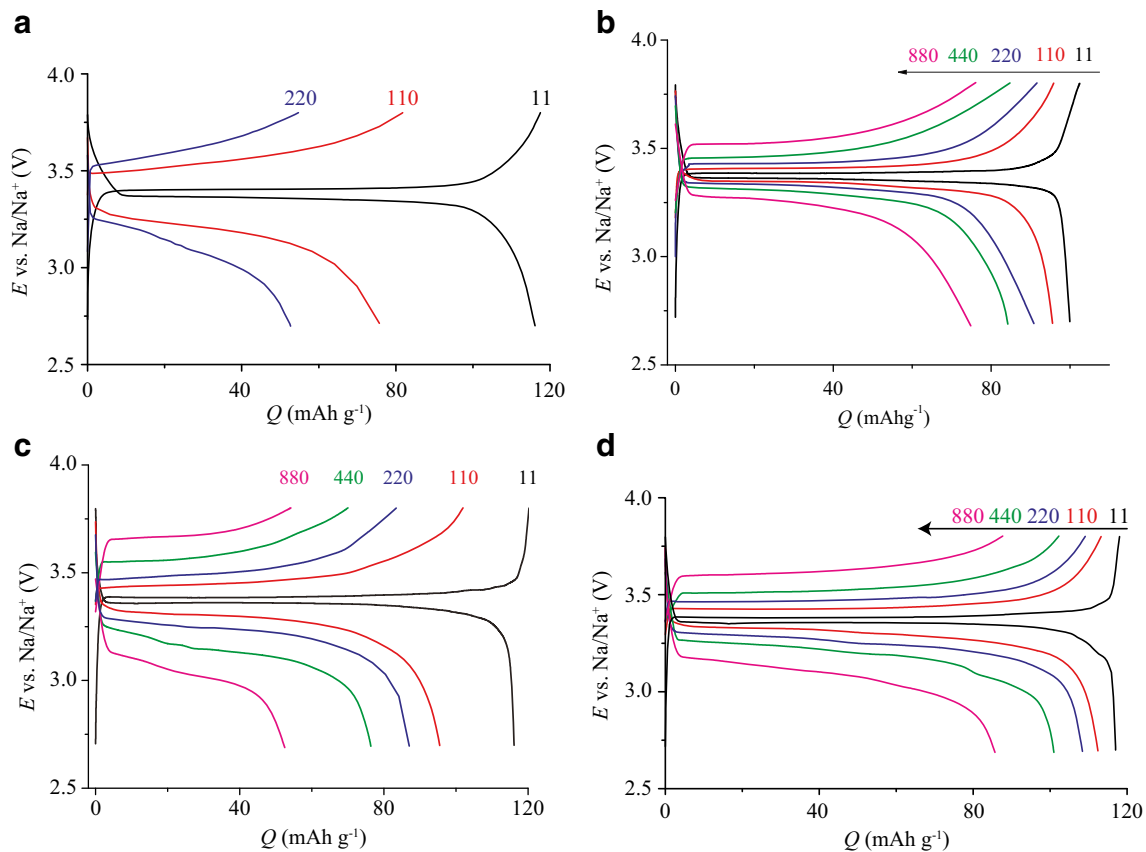


**Fig. 6** Charge-discharge curves for NVP/C-600 (a), NVP/C/Ag-600 (b), NVP/C-600-800 (c), and NVP/C/Ag-600-800 (d). Current densities (mA g<sup>-1</sup>) are noted near curves

**Table 2** Discharge capacity of NVP/C/xAg materials depending on the preparation condition and Ag content at different current densities (mA g<sup>-1</sup>). The conductivity of the samples is presented as well

Sample	Ag content (x), wt%	Discharge capacity at I = 11 mA g <sup>-1</sup> (0.1C)	Discharge capacity at I = 110 mA g <sup>-1</sup> (1C)	Discharge capacity at I = 880 mA g <sup>-1</sup> (8C)	σ, S cm <sup>-1</sup>
NVP/C-600	–	116.1	75.0	–	2.1*10 <sup>-5</sup>
NVP/C-800	–	100.1	29.3	–	1.3*10 <sup>-1</sup>
NVP/C-600-800	–	117.1	90	52.4	1.7*10 <sup>-2</sup>
NVP/C/xAg-600	0.2	100.0	67.9	52.2	2.9*10 <sup>-5</sup>
NVP/C/xAg-600	2	73.3	70.8	58.2	3.5*10 <sup>-5</sup>
NVP/C/xAg-600	5	63.5	61.5	48.4	3.6*10 <sup>-5</sup>
NVP/C/xAg – 600-800	0.2	117.2	112.5	83.5	3.1*10 <sup>-2</sup>
NVP/C/xAg – 600-800	2	95.6	91.4	69.7	4.1*10 <sup>-2</sup>

mAh g<sup>-1</sup> at current densities of 11 (0.1C), 110 (1C), and 880 mA g<sup>-1</sup> (8C) (Fig. 6d, Fig. 7).

Upon NVP/C-600 charge-discharge cycling, the discharge capacity decreases by about 0.1% per cycle (at 11 mA g<sup>-1</sup>) upon 100 cycles. The capacity of NVP/C/0.2Ag-600-800 decreases by about 0.02% per cycle at a current density 11 mA g<sup>-1</sup> and about 0.05% per cycle at a current density 880 mA g<sup>-1</sup> upon 100 cycles. Also, it should be mentioned that the capacities of NVP/C/-600-800 and NVP/C/0.2Ag-600-800 recovered to the initial value after charge-discharge cycle at low current density (Fig. 7). So, one can conclude that cycling performance of NVP/C was improved after short heat treatment at 800 °C and silver addition to the composite.

Figure 8a, b shows cyclic voltammograms for NVP/C-600 and NVP/C/Ag-600-800 with Ag content of 0.2 wt% recorded at different potential scan rates (ν). Every curve contains two well-pronounced redox peaks: the anode peak corresponds to the extraction of Na<sup>+</sup> ions, and the cathode peak to the intercalation of Na<sup>+</sup> ions. The potential scan rate, which is equal to 0.1 mV s<sup>-1</sup>, approximately corresponds to the 5-h charge-discharge regime. The discharge capacity was calculated from the area under the cathode region of the voltammetric curve; this value is equal to 97, 85, and 72 mAh g<sup>-1</sup> for NVP/C-600 and 116, 108, and 102 mAh g<sup>-1</sup> for NVP/C/Ag-600-800 sample at a potential scan rate of 0.1, 0.2, and 0.4 mV s<sup>-1</sup>, respectively. This correlates with the data of galvanostatic measurements. Figure 8c represents the comparison of cyclic voltammograms for NVP/C-600 and NVP/C/Ag-600-800 at 0.1 mV s<sup>-1</sup> and illustrates the considerably increase in the maximums of cathodic and anodic peak currents for NVP/C/Ag-600-800.

The dependence of the peak current (I<sub>p</sub>) on the square root of potential scan rate (ν<sup>1/2</sup>) is linear and passes through the origin of coordinates (Fig. 8d). Hence, one can calculate the effective diffusion coefficient of sodium ions (D<sub>eff</sub>) in NVP/C according to the Randels-Ševčík equation:

$$I_p = 2.69 \times 10^5 n^{3/2} S \times D^{1/2}_{Na} \nu^{1/2} c \tag{1}$$

where I<sub>p</sub> is the peak current (A), n is the number of electrons in the reaction cycle, S is the electrode surface area (cm<sup>2</sup>), c is the concentration of sodium ions in NVP/C (mol cm<sup>-3</sup>), ν is the potential scan rate (V s<sup>-1</sup>), and D is the diffusion coefficient of sodium ions in NVP/C (cm<sup>2</sup> s<sup>-1</sup>).

The slope dI<sub>p</sub>/dν<sup>1/2</sup> estimated from the plots in Fig. 8d is equal to 0.027 and 0.025 A V<sup>-1/2</sup> s<sup>1/2</sup> for NVP/C-600 for anodic and cathodic peaks, respectively. At the same time, the slope increases in the order of magnitude for NVP/C/Ag-600-800 and is equal to 0.273 and 0.342 A V<sup>1/2</sup> s<sup>1/2</sup> for anodic and cathodic peaks, respectively. This fact points to the considerable improvement (eq. (1)) of sodium diffusivity for NVP/C/Ag-600-800. Sodium diffusivity was estimated by the Randles-Sevcik model. Concentration of sodium ions was calculated from the

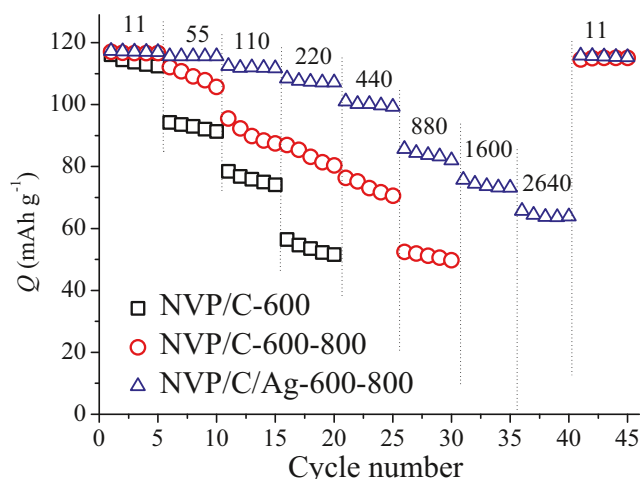


**Fig. 7** Changes in specific discharge capacity at different current densities for NVP/C-600, NVP/C-600-800, and NVP/C/Ag-600-800. Current densities (mA g<sup>-1</sup>) are presented

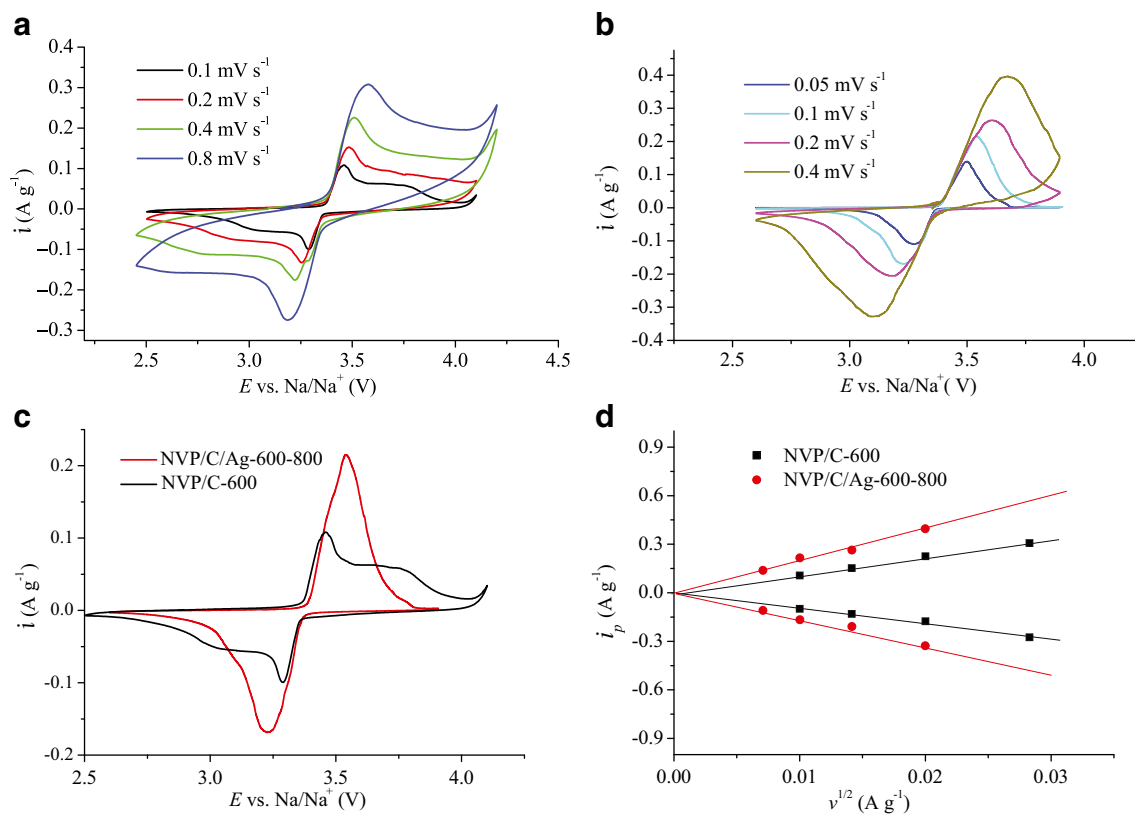


**Fig. 8** Cyclic voltammograms of the NVP/C-600 (a) and NVP/C/Ag-600-800 (b) electrodes at different potential scanning rates; cyclic voltammogram of the NVP/C-600 and NVP/C/Ag-600-800 electrodes at the

scanning rate of 0.1 mV s<sup>-1</sup> (c); and anodic and cathodic peak currents plotted against the square root of the potential scanning rate for NVP/C-600 and NVP/C/Ag-600-800 (d)

capacity and weight of NVP/C on the electrode; this value is equal to  $9.3 \cdot 10^{-3}$  mol cm<sup>-3</sup> for NVP/C-600 and  $13.5 \cdot 10^{-3}$  mol cm<sup>-3</sup> for NVP/C/Ag-600-800. In literature, there is no uniform opinion about the electrode surface area that should be taken for the calculation using the Randles-Sevcik model. Diffusion coefficients can differ by several orders of magnitude if one selects surface area of electrode which was estimated from the low-temperature nitrogen sorption or geometric surface area [12] or calculated from the averaged radius of aggregated particles estimated from the electron microscopy data [45, 46]. The last choice, for us, seems more appropriate because it assumes that diffusion rate is determined by the Na<sup>+</sup> transfer in agglomerates that consist of primary NVP particles coated with carbon. Transfer between the particles is faster due to the fact that it occurs in carbon layer. In this case, the effective diffusion coefficient of sodium ions is equal to  $7.5 \times 10^{-14}$  and  $6.7 \times 10^{-14}$  cm<sup>2</sup> s<sup>-1</sup> for NVP/C-600 and  $1.28 \times 10^{-12}$  and  $1.14 \times 10^{-12}$  cm<sup>2</sup> s<sup>-1</sup> for NVP/C/Ag-600-800 for intercalation and extraction of sodium ions, respectively. So, we observed sodium diffusivity improvement as a result of carbon-coating development by post heat treatment and silver incorporation into composites.

## Conclusions

In this work, the carbon-coated nanocomposite cathode materials based on NVP with the rhombohedral NASICON structure and silver nanoparticles introduction were prepared by the modified Pechini method. It was shown that it allows to prepare crystalline NVP/C materials at 600 °C. The discharge capacity of NVP/C obtained at 600 °C was 116.1 and 75 mAh g<sup>-1</sup> at a current density of 11 (0.1 C) and 110 mA g<sup>-1</sup> (1 C) in a potential range of 2.7–3.8 V. As a result of optimization of heat treatment conditions and appropriate amount of silver particle incorporation into NVP/C composite, high capacity values for fast charge/discharge were obtained. The discharge capacities of NVP/C/Ag with 0.2 wt% of Ag first annealed at 600 °C and follow heated at 800 °C were 117.2, 112.5, and 83.5 mAh g<sup>-1</sup> at current densities of 11, 110, and 880 mA g<sup>-1</sup>. This experimental evidence reveals the great potential of NVP/C/Ag synthesized by the modified Pechini method as cathode materials for the production of sodium-ion batteries.

**Acknowledgments** This work was financially supported by the Russian Foundation for Basic Research and Moscow Government (project no. 15-38-70042). In this work, we used the equipment of the Joint Research Center of IGIC RAS.



## References

- Palomares V, Serras P, Villaluenga I, Hueso KB, Carretero-González J, Rojo T (2012) Na-ion batteries, recent advances and present challenges to become low cost energy storage systems. *Energy Environ Sci* 5:5884–5901
- Pan H, Hu YS, Chen L (2013) Room-temperature stationary sodium-ion batteries for large-scale electric energy storage. *Energy Environ Sci* 6:2338–2360
- Slater MD, Kim D, Lee E, Johnson CS (2013) Sodium-ion batteries. *Adv Funct Mater* 23:947–958
- Kim SW, Seo DH, Ma X, Ceder G, Kang K (2012) Electrode materials for rechargeable sodium-ion batteries: potential alternatives to current lithium-ion batteries. *Adv Energy Mater* 2:710–721
- Sudworth JL (1984) The sodium/sulphur battery. *J Power Sources* 11:143–154
- Dustmann CH (2004) Advances in ZEBRA batteries. *J Power Sources* 127:85–92
- Yabuuchi N, Kubota K, Dahbi M, Komaba S (2014) Research development on sodium-ion batteries. *Chem Rev* 114:11636–11682
- Li H, Bai Y, Wu F, Li Y, Wu C (2015) Budding willow branches shaped  $\text{Na}_3\text{V}_2(\text{PO}_4)_3/\text{C}$  nanofibers synthesized via an electrospinning technique and used as cathode material for sodium ion batteries. *J Power Sources* 273:784–792
- Lim SY, Kim H, Shakoor RA, Jung Y, Choi JW (2012) Electrochemical and thermal properties of NASICON structured  $\text{Na}_3\text{V}_2(\text{PO}_4)_3$  as a sodium rechargeable battery cathode: a combined experimental and theoretical study. *J Electrochem Soc* 159: A1393–A1397
- Song W, Ji X, Pan C, Zhu Y, Chen Q, Banks CE (2013) A  $\text{Na}_3\text{V}_2(\text{PO}_4)_3$  cathode material for use in hybrid lithium ion batteries. *Phys Chem Chem Phys* 15:14357–14363
- Song W, Ji X, Yao Y, Zhu H, Chen Q, Sun Q, Banks CE (2014) A promising  $\text{Na}_3\text{V}_2(\text{PO}_4)_3$  cathode for use in the construction of high energy batteries. *Phys Chem Chem Phys* 16:3055–3061
- Song W, Ji X, Wu Z, Zhu Y, Yang Y, Chen J, Jing M, Li F, Banks CE (2014) First exploration of Na-ion migration pathways in the NASICON structure  $\text{Na}_3\text{V}_2(\text{PO}_4)_3$ . *J Mater Chem A* 2:5358–5362
- Jung YH, Lim Ch H, Kim DK (2013) Graphene-supported  $\text{Na}_3\text{V}_2(\text{PO}_4)_3$  as a high rate cathode material for sodium-ion batteries. *J Mater Chem A* 1:11350–11354
- Goodenough JB, Hong HYP, Kafalas JA (1976) Fast  $\text{Na}^+$ -ion transport in skeleton structures. *Mater Res Bull* 11:203–220
- Saravanan K, Mason CW, Rudola A, Wong KH, Balaya P (2013) The first report on excellent cycling stability and superior rate capability of  $\text{Na}_3\text{V}_2(\text{PO}_4)_3$  for sodium ion batteries. *Adv Energy Mater* 3:444–450
- Zhu X, Fang Y, Ai X, Yang H, Cao Y (2015)  $\text{Na}_3\text{V}_2(\text{PO}_4)_3/\text{C}$  nanocomposite synthesized via pre-reduction process as high-performance cathode material for sodium-ion batteries. *J Alloys Compd* 646:170–174
- Plashnitsa LS, Kobayashi E, Noguchi Y, Okada S (2010) Yamaki JI. Performance of NASICON Symmetric Cell with Ionic Liquid Electrolyte *J Electrochem Soc* 157:A536–A543
- Si L, Yuan Zh HL, Zhu Y, Qian Y (2014) Uniform and continuous carbon coated sodium vanadium phosphate cathode materials for sodium-ion battery. *J Power Sources* 272:880–885
- Zhu X, Fang Y, Ai X, Yang H, Cao Y (2015)  $\text{Na}_3\text{V}_2(\text{PO}_4)_3/\text{C}$  nanocomposite synthesized via pre-reduction process as high-performance cathode material for sodium-ion batteries. *J Alloys Compd* 646:170–174
- Li S, Dong YF, Xu L, Xu X, He L, Mai LQ (2014) Batteries: effect of carbon matrix dimensions on the electrochemical properties of  $\text{Na}_3\text{V}_2(\text{PO}_4)_3$  nanograins for high-performance symmetric sodium-ion batteries. *Adv Mater* 26:3545–3553
- Aragon MJ, Lavela P, Ortiz GF, Tirado JL (2015) Effect of iron substitution in the electrochemical performance of  $\text{Na}_3\text{V}_2(\text{PO}_4)_3$  as cathode for Na-ion batteries. *J Electrochem Soc* 162:A3077–A3083
- Liu J, Tang K, Song KP, Aken PAV, Yu Y, Maier J (2014) Electrospun  $\text{Na}_3\text{V}_2(\text{PO}_4)_3/\text{C}$  nanofibers as stable cathode materials for sodium-ion batteries. *Nanoscale* 6:5081–5086
- Li GQ, Jiang DL, Wang H, Lan XZ, Zhong HH, Jiang Y (2014) Glucose-assisted synthesis of  $\text{Na}_3\text{V}_2(\text{PO}_4)_3/\text{C}$  composite as an electrode material for high-performance sodium-ion batteries. *J Power Sources* 265:325–334
- Shen W, Wang C, Liu HM, Yang WS (2013) Towards highly stable storage of sodium ions: a porous  $\text{Na}_3\text{V}_2(\text{PO}_4)_3/\text{C}$  cathode material for sodium-ion batteries. *Chem Eur J* 19:14712–14718
- Zhu CB, Song KP, Aken PAV, Yu Y, Maier J (2014) Carbon-coated  $\text{Na}_3\text{V}_2(\text{PO}_4)_3$  embedded in porous carbon matrix: an ultrafast Na-storage cathode with the potential of outperforming Li cathodes. *Nano Lett* 14:2175–2180
- Chen M, Kou K, Tu M, Hu J, Yang B. g (2015) Fabrication of multi-walled carbon nanotubes modified  $\text{Na}_3\text{V}_2(\text{PO}_4)_3/\text{C}$  and its application to high-rate lithium-ion batteries cathode *Solid State Ionics* 274:24–28
- Chu Zh, Yue C (2016) Core-shell structured  $\text{Na}_3\text{V}_2(\text{PO}_4)_3/\text{C}$  nanocrystals embedded in multi-walled carbon nanotubes: a high-performance cathode for sodium-ion batteries *Solid State Ionics* 287:36–41.
- Wang KX, Li XH, Chen JS (2015) Surface and interface engineering of electrode materials for lithium-ion batteries. *Adv Mater* 27: 527–545
- Gryzlov D, Novikova S, Kulova T, Skundin A, Yaroslavtsev A (2016) Behavior of  $\text{LiFePO}_4/\text{C}_{\text{PVDF}}/\text{Ag}$ -based cathode materials obtained using polyvinylidene fluoride as the carbon source. *Mater Des* 104:95–101
- Jian Z, Zhao L, Pan H, Hu YS, Li H, Chen W, Chen L (2012) Carbon coated  $\text{Na}_3\text{V}_2(\text{PO}_4)_3$  as novel electrode material for sodium ion batteries. *Electrochem Commun* 14:86–89
- Wang H, Jiang D, Zhang Y, Li G, Lan X, Zhong H, Zhang Z, Jiang Y (2015) Self-combustion synthesis of  $\text{Na}_3\text{V}_2(\text{PO}_4)_3$  nanoparticles coated with carbon shell as cathode materials for sodium-ion batteries. *Electrochim Acta* 155:23–28
- Zhang Y, Zhao H, Du Y (2016) Symmetric full cell assembled by self-supporting  $\text{Na}_3\text{V}_2(\text{PO}_4)_3$  bipolar electrodes for superior sodium energy storage. *J Mater Chem A* 4:7155–7159
- Fang J, Wang S, Li Z, Chen H, Xia L, Ding L, Wang H (2016) Porous  $\text{Na}_3\text{V}_2(\text{PO}_4)_3@C$  nanoparticles enwrapped in three-dimensional graphene for high performance sodium-ion batteries. *J Mater Chem A* 4:1180–1185
- Tao S, Cui P, Huang W, Yu Z, Wang X, Liu D, Song L, Chu W, Wei S (2016) Sol-gel design strategy for embedded  $\text{Na}_3\text{V}_2(\text{PO}_4)_3$  particles into carbon matrices for high-performance sodium-ion batteries. *Carbon* 96:1028–1033
- Wang D, Chen N, Li M, Wang C, Ehrenberg H, Bie X, Wei Y, Chen G, Du F (2015)  $\text{Na}_3\text{V}_2(\text{PO}_4)_3/\text{C}$  composite as the intercalation-type anode material for sodium-ion batteries with superior rate capability and long-cycle life. *J Mater Chem A* 3:8636–8642
- Vidano RP, Fishbach DB (1981) Observation of Raman band shifting with excitation wavelength for carbons and graphites. *Solid State Comm* 39:341–344
- Xie W, Zhu X, Yi S, Kuang J, Cheng H, Tang W, Deng Y (2016) Electromagnetic absorption properties of natural microcrystalline graphite. *Mater Des* 90:38–46

38. Wilcox JD, Doeff MM, Marcinek M, Kostecki R (2007) Factors influencing the quality of carbon coatings on  $\text{LiFePO}_4$ . *J Electrochem Soc* 154:A389–A395
39. Bhuvaneswari MS, Bramnik NN, Ensling D, Ehrenberg H, Jaegermann W (2008) Synthesis and characterization of carbon nano fiber/ $\text{LiFePO}_4$  composites for Li-ion batteries. *J Power Sources* 180:553–560
40. Doeff MM, Hu Y, F. McLarnon, Kostecki R (2003) Effect of surface carbon structure on the electrochemical performance of  $\text{LiFePO}_4$ . *Electrochem Solid-State Lett* 6:A207–A209
41. Bonhomme F, Lassegues JC, Servant L (2001) Raman spectroelectrochemistry of a carbon supercapacitor. *J Electrochem Soc* 148:E450–E458
42. Mariappan CR, Galven C, Crosnier-Lopez MP, Le Berre F, Bohnke O (2006) Synthesis of nanostructured  $\text{LiTi}_2(\text{PO}_4)_3$  powder by a Pechini-type polymerizable complex method. *J Solid State Chem* 179:450–456
43. Ejehi F, Marashi SPH, Ghaani MR, Haghshenas DF (2012) The synthesis of NaSICON-type  $\text{ZrNb}(\text{PO}_4)_3$  structure by the use of Pechini method. *Ceram Int* 38:6857–6863
44. Il'in AB, Novikova SA, Sukhanov MV, Ermilova MM, Orekhova NV, Yaroslavtsev AB (2012) Catalytic activity of NASICON-type phosphates for ethanol dehydration and dehydrogenation. *Inorg Mater* 48:397–401
45. Vujković M, Stojković I, Cvjetičanin N, Mentus S (2013) Gel-combustion synthesis of  $\text{LiFePO}_4/\text{C}$  composite with improved capacity retention in aerated aqueous electrolyte solution. *Electrochim Acta* 92:248–256
46. Li P, Shao L, Wang P, Zheng X, Yu H, Qian Sh, Shui M, Long N, Shu J (2015) Lithium sodium vanadium phosphate and its phase transition as cathode material for lithium ion batteries. *Electrochim Acta* 180:120–128